International Forum on Aeroelasticity and Structural Dynamics
IFASD 2024
17-21 June 2024, The Hague, The Netherlands

PREDICTION OF TRANSONIC BUFFET IN AN AXIAL FLOW FAN USING GLOBAL STABILITY ANALYSIS

Jyoti Ranjan Majhi[1] **and Kartik Venkatraman**[1]

[1]Indian Institute of Science
Bangalore, India, 560012
jyotir@iisc.ac.in
kartik@aero.iisc.ac.in

Keywords: Transonic flow, shock buffet, global stability analysis

Abstract: Shock oscillation arising due to shock-boundary layer interaction in transonic flow, also known as transonic buffet, gives rise to time varying airloads on fan and compressor blades, which can lead to failure of the concerned component through fatigue. Therefore, accurate estimates of the onset of transonic buffet, shock displacement, and buffet frequency are critical to lifing assessment of turbomachinery blades. In the present work, we use a global stability framework for transonic flow to predict transonic shock buffet in an axial flow fan, the NASA rotor 67. Global stability analysis of fluid flow involves investigation of the behavior of a steady or mean flow field, also known as base flow, upon introduction of small three-dimensional perturbations, in terms of growth or decay of the resulting flow field. In this work, aerodynamic stability of the flow field is predicted at an operating point on the fan operating map, where buffet is reported, using global stability analysis, and the prediction obtained so is compared vis-à-vis the prediction obtained using unsteady Reynolds-averaged Navier-Stokes (URANS) simulation.

1 INTRODUCTION

Transonic shock buffet or self-sustained shock oscillation in transonic flow gives rise to time-varying pressure fluctuations on gas turbine fan and compressor blades, thus causing unsteady aerodynamic loading that can trigger structural vibration, also known as buffeting, which in turn can potentially lead to fatigue and failure of the concerned component. Accurate estimates of the onset of transonic buffet, shock displacement, and buffet frequency are critical to assess the extent of unsteady loading on turbomachinery blades undergoing transonic buffet.

Shock-boundary layer interaction with boundary layer separation and shock oscillation during transonic flight is well-investigated in fixed wings [1–5]. Reviews of literature over the past two decades record the progress made in understanding this phenomenon using both wind tunnel experiments and high fidelity numerical investigations [6–8].

In turbomachinery, there is a dearth of literature that have studied transonic buffet. Reference [9] investigated shock structure and shock oscillations of a transonic fan, NASA rotor 67, using laser anemometry data. References [10, 11] investigated shock-boundary layer interactions and shock oscillations in a compressor cascade (non-rotating) consisting of six blades placed in a transonic flow. Recently, Ref. [12] simulated transonic buffet on NASA rotor 67 near design mass flow operating point using URANS and reported of pressure waves circumferentially traveling at part-speed of fan speed in the spinning direction of the fan found from modal

decomposition of buffet flow. More recently, Ref. [13] tried to explain the buffet mechanism in NASA rotor 67 at design mass flow with the help of wave propagation analysis of buffet flow.

Researchers have tried to explain the mechanism of shock buffet using broadly three types of analyses—1) wave propagation analysis [1–3, 6, 14], 2) modal analysis of flow [15–17], and global stability analysis [18–20]. With advancements in computational power and numerical methods, global stability analysis has been a powerful tool for studying shock buffet on three-dimensional wings. Techniques like the Krylov methods employing the shift-and-invert strategy (Krylov-Schur [21] and ARPACK [22]) have made it possible to solve large-scale eigenvalue problems associated with realistic wing geometries. Global stability analysis stands out for its ability to provide detailed quantitative and qualitative insights into the mechanisms of transonic shock buffet. Its comprehensive perspective on flow behavior, predictive capabilities, versatility, and integration with computational methods make it a superior tool for researchers aiming to understand and mitigate shock buffet in aerodynamic applications. Global stability analysis involves examining the linear stability of a base flow to understand the onset and development of flow instabilities. It uses the Navier-Stokes equations linearized around a steady or time-averaged (mean) flow solution. By solving the eigenvalue problem, resulting of the linearization, one can identify unstable modes and their growth rates, providing insights into the mechanisms driving flow instabilities.

While there is appreciable amount of literature available on the use of global stability analysis on wings and wing-sections to study shock buffet, there is hardly any in the realm of turbomachinery. In this work, we intend to capture and understand the underlying flow physics of a transonic fan undergoing shock buffet using global stability analysis.

2 TESTCASE

The test case chosen for this work is a transonic axial-flow fan—the NASA rotor 67. Experimental data for steady state performance of rotor 67 including geometry details are available in [23, 24]. The rotor 67 has 22 low aspect ratio blades with a design rotational speed of 16043 rev/min, a design mass flow rate of 33.25 Kg/s, and a design pressure ratio of 1.63. The design rotor tip speed is 429 m/s and the design tip clearance is 0.001016 m. Figure 1 shows

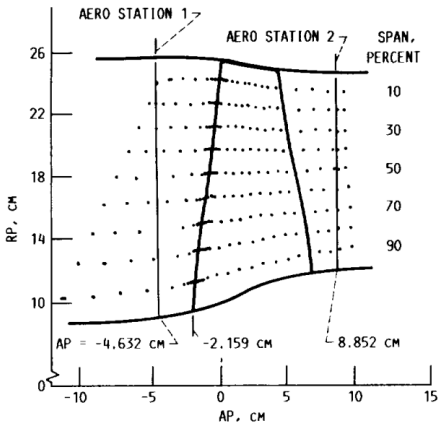

Figure 1: Meridional view of NASA rotor 67 and aerodynamic survey locations [23].

the meridional view of the configuration and aerodynamic survey locations (AERO STATIONS 1 and 2) where relevant flow variables are sampled for evaluating the fan performance parameters [23].

For this fan configuration shock oscillations were reported from laser anemometry observations [23], and the authors have simulated transonic buffet using URANS earlier [13]. In the present work, we aim to predict the unsteady flow field during shock buffet using global stability analysis.

3 COMPUTATIONAL METHODS

3.1 Numerical method for fluid flow simulation

3.1.1 Governing equations

The Stanford University Unstructured or SU2 [25, 26] suite of computer codes for solving Reynolds-averaged Navier-Stokes (RANS) and URANS equations is used to obtain fluid flow solutions. SU2 is a cell-vertex based finite volume solver. The system of governing equations in conservative form for a domain $\Omega \subset \mathbb{R}^3$ in compressible viscous flow is given by

$$\mathcal{R}(\boldsymbol{U}) = \frac{\partial \boldsymbol{U}}{\partial t} + \boldsymbol{\nabla} \cdot \boldsymbol{F}_c - \boldsymbol{\nabla} \cdot \boldsymbol{F}_v - \boldsymbol{Q} = \boldsymbol{0}, \quad \text{in} \quad \Omega, \quad t > 0. \tag{1}$$

where $\boldsymbol{U} = [\rho,\, \rho\boldsymbol{q},\, \rho E]^T$ is the vector of conservative variables with ρ denoting the fluid density, $\boldsymbol{q}$ is the flow velocity in the rotating frame of reference, and E is the relative total energy per unit mass [27, 28]. $\boldsymbol{F}_c$ is the vector of convective fluxes, $\boldsymbol{F}_v$ is the vector of viscous fluxes and $\boldsymbol{Q}$ is the vector of source terms in the rotating frame of reference given by

$$\boldsymbol{F}_c = \begin{bmatrix} \rho\boldsymbol{q} \\ \rho\boldsymbol{q} \otimes \boldsymbol{q} + \bar{\bar{\boldsymbol{I}}}p \\ \rho\boldsymbol{I}\boldsymbol{q} \end{bmatrix}, \quad \boldsymbol{F}_v = \begin{bmatrix} 0 \\ \bar{\bar{\boldsymbol{\tau}}} \\ \bar{\bar{\boldsymbol{\tau}}} \cdot \boldsymbol{q} + \mu_{tot} c_p \boldsymbol{\nabla} T \end{bmatrix},$$

$$\boldsymbol{Q} = \begin{bmatrix} 0 \\ \rho(\boldsymbol{f} + \boldsymbol{f}_{cor} + \boldsymbol{f}_{cent}) \\ \rho\boldsymbol{f} \cdot \boldsymbol{q} + \boldsymbol{q}_H \end{bmatrix}$$

with $\boldsymbol{I} = h + \frac{\boldsymbol{q}^2}{2} - \frac{\boldsymbol{u}^2}{2}$ denoting the rothalpy for systems referenced in a rotating frame where, h is the enthalpy of the system and $\boldsymbol{u} = \boldsymbol{\Omega} \times \boldsymbol{r}$ is the entrainment velocity, $\boldsymbol{\Omega}$ and $\boldsymbol{r}$ being the rotational speed of the rotating frame and the position vector respectively, and $\bar{\bar{\boldsymbol{I}}}$ is the unit tensor and p is the pressure. $\mu_{tot} = \frac{\mu_{lam}}{Pr_{lam}} + \frac{\mu_{tur}}{Pr_{tur}}$ is the non-dimensional viscosity, Pr_{lam} and Pr_{tur} being the laminar and turbulent Prandtl numbers respectively, and c_p is the specific heat at constant pressure and T is the temperature. The turbulent viscosity μ_{tur} is derived using a suitable turbulence model. The viscous stress tensor $\bar{\bar{\boldsymbol{\tau}}}$ is given as

$$\bar{\bar{\boldsymbol{\tau}}} = \mu_{tot}\left(\boldsymbol{\nabla}\boldsymbol{q} + \boldsymbol{\nabla}\boldsymbol{q}^T - \frac{2}{3}\boldsymbol{\nabla}.\boldsymbol{q}\bar{\bar{\boldsymbol{I}}}\right)$$

The term $\boldsymbol{f}$ is the external force (per unit volume) vector and the additional terms $\boldsymbol{f}_{cor} = -2(\boldsymbol{\Omega} \times \boldsymbol{q})$ and $\boldsymbol{f}_{cent} = -\boldsymbol{\Omega} \times (\boldsymbol{\Omega} \times \boldsymbol{r})$ are the Coriolis and centrifugal forcing terms respectively that appear when the frame of reference is rotating with an angular velocity $\boldsymbol{\Omega}$, and $\boldsymbol{q}_H$ is the external heat source. The pressure is related to the velocities and energy through the equation of state.

3.1.2 Numerical schemes

The governing partial differential equations Eq. 1 are solved using a cell-vertex based finite volume scheme [28] where the variables are evaluated at the vertices of the constituent subdomains. The convective fluxes are discretized using a Roe upwind scheme [29] and second

order MUSCL reconstruction was achieved using the Van Albada limiter [30]. The viscous terms were discretized using an average-gradient formulation. The gradients were evaluated using a lest-squares method [27] at all nodes and subsequently approximating that at the cell faces. The source terms are approximated using piece-wise constant reconstruction within each of the finite volume cells.

The spatially discretized equations are temporally discretized and integrated using the Euler implicit method. It employs the generalized minimum residual (GMRES) method which approximates the solution by the vector in a Krylov subspace with minimal residual, found by Arnoldi iteration. An incomplete Lower-Upper (ILU) factorization scheme is employed for pre-conditioning the linear solver.

A Courant–Friedrichs–Lewy (CFL) number of 20 was chosen for the steady state simulations.

3.1.3 Turbulence model

The Spalart-Allmaras (SA) turbulence model [31] with Edwards and Chandra's correction [32] is used for carrying out all simulations presented in this paper. The choice of this variant of the SA turbulence model is driven by the fact that transonic buffet on supercritical airfoils [15, 33] and on three-dimensional fixed wing [34] is successfully simulated using this turbulence model. The Edwards and Chandra's correction improves the near-wall behaviour of the standard SA model. This turbulence model tries to address the failure of eddy-viscosity based turbulence models to induce the correct rate of boundary-layer recovery following separation, and thus is able to predict shock buffet which involves intermittent boundary-layer separation and reattachment.

The standard SA model maintains the log-layer behavior of the strain-rate norm all the way to the wall and displays singular behaviour for it in the near-wall region. With alternative formulations for the strain-rate norm and the argument of the wall-blockage function, the version of SA turbulence model by Edwards and Chandra gives a more stable way of accounting for the behavior of the strain-rate norm in the laminar sub-layer with better convergence when compared with the standard SA model.

3.1.4 Boundary conditions

For the flow, total pressure and total temperature are specified at the inlet as boundary conditions. At the exit, suitable static/back pressure is applied as boundary condition to achieve the desired mass flow rate. No-slip and adiabatic boundary conditions are applied to the solid walls. The flow boundary conditions for the chosen test case, taken from Ref. [23], are presented in Table 1.

Table 1: Boundary conditions

Boundary	Description
Inlet	Total Pressure (101325 Pa)
	Total Temperature (288.15 K)
Outlet	Static pressure/back pressure

3.1.5 Computational grid

The extents of a periodic sector consisting of a single passage of the computational domain used along with a picture of the full-annulus mesh is shown in Fig. 2. The inlet is chosen to be at an axial location one and half times the axial chord upstream of the blade leading edge at hub and the outlet is chosen to be at an axial location twice the axial chord downstream of the blade trailing edge at hub. The flow domain was discretized with a H-O-H type of grid using Autogrid5 Academic software. The full-annulus mesh was constructed by duplicating the single-passage mesh 22 times.
A grid consisting of 0.81 million cells per blade passage was selected following a grid convergence study based on steady state performance that included two more grids with cell counts of 0.4 and 1.6 million cells. The chosen grid consists of 117 and 57 divisions in the axial and circumferential directions respectively. The blade surface mesh consists of 75 elements in the span-wise direction. The mesh surrounding the blade surface consists of 17 O-grids and the mesh beyond that consists of H-grids. 17 span-wise cells are used for generating the tip gap region mesh which is surrounded by 15 O-grids. The y^+ values were kept with in the upper bound of 1 at the blade, hub and shroud surfaces. More details on the computational grid can be found in [13].

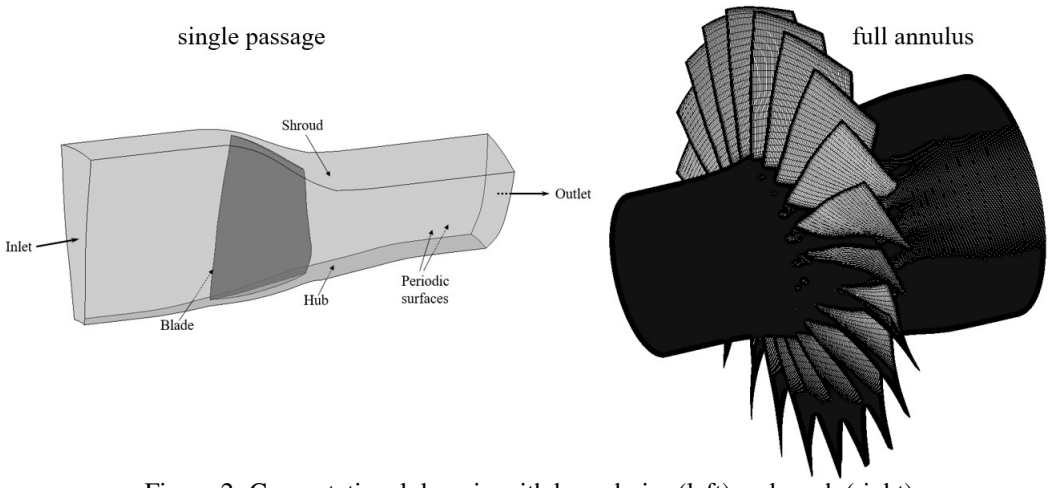

Figure 2: Computational domain with boundaries (left) and mesh (right)

3.2 Global stability analysis

Global stability analysis involves investigation of the behavior of a steady or mean flow field, also known as base flow, upon introduction of small three-dimensional perturbations, in terms of growth or decay of the resulting flow field. The governing Eq.(1), after spatial discretization, can be written as

$$\frac{\mathrm{d}\boldsymbol{U}}{\mathrm{d}t} = \mathcal{R}(\boldsymbol{U}) \tag{2}$$

If there exists a base flow $\mathbf{U}_b$, then $\mathcal{R}(\mathbf{U}_b) = 0$ as the base flow is stationary by definition. To assess the stability of the base flow, a small perturbation $\mathbf{U}'$ is applied to the base flow $\mathbf{U}_b$ so that the resulting perturbed flow is $\mathbf{U} = \mathbf{U}_b + \mathbf{U}'$. After linearizing the discretized Eq.(2) to first order, the governing equation for the perturbation can be written as

$$\frac{\mathrm{d}\boldsymbol{U}'}{\mathrm{d}t} = \boldsymbol{J}\boldsymbol{U}' \tag{3}$$

where $\boldsymbol{J} = \frac{\partial \mathcal{R}}{\partial \boldsymbol{U}}\big|_{\mathbf{U}=\mathbf{U}_b}$ is the Jacobian corresponding to the linearization of the residual $\mathcal{R}$ around the base flow $\mathbf{U}_b$. Assuming a solution of the form $\boldsymbol{U}'(x, y, z, t) = \widehat{\boldsymbol{U}}(x, y, z)e^{\lambda t}$, Eq.(3) can be written as an eigenvalue problem as follows.

$$\boldsymbol{J}\widehat{\boldsymbol{U}} = \lambda \widehat{\boldsymbol{U}} \tag{4}$$

where $\widehat{\boldsymbol{U}}$ are the global modes and $\lambda = \sigma + i\omega$ are the eigenvalues, σ and ω representing the growth rate and frequency (angular) of the global modes respectively. The base flow becomes unstable when at least one of the global modes exhibits a positive growth rate.
Elements of the Jacobian corresponding to a stencil usually depend only on the variables within the immediate neighbourhood of the particular stencil. Thus the Jacobian is usually a sparse matrix. The eigenvalue problem Eq.(4) is solved using SLEPc (Scalable Library for Eigenvalue Problem Computations) and PETSc (Portable, Extensible Toolkit for Scientific Computation). The Krylov-Schur [21] algorithm is used for solving the eigenvalue problem with a shift-and-invert strategy. The distributed direct sparse lower-upper (LU) solver MUMPS (**MU**ltifrontal **M**assively **P**arallel sparse direct **S**olver) is employed for matrix inversion. The computations are carried out on a cluster based on 48-core Intel Xeon Cascade Lake 8268 2.9 GHz processors with 192 GB RAM.

4 RESULTS AND DISCUSSIONS

The fan configuration considered exhibits shock oscillations in the vicinity of the design mass flow operating point on the fan performance map. We have investigated buffet flow near the design mass flow operating point. Figures 3 and 4 show relative Mach contours with constant Mach lines at 70% and 90% span respectively for the chosen operating point. A detached bow

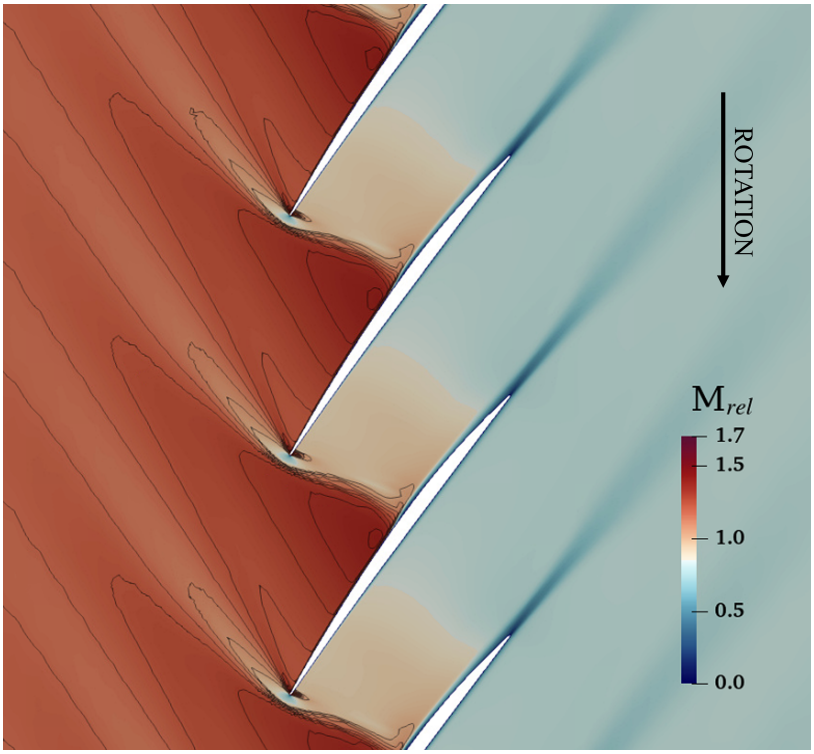

Figure 3: Steady flow results - Relative Mach contours with constant Mach lines at 70% span

shock is seen in these figures which is merged with the passage shock present on the suction surface. The foot of the passage shock is distorted due to boundary layer growth on the suction

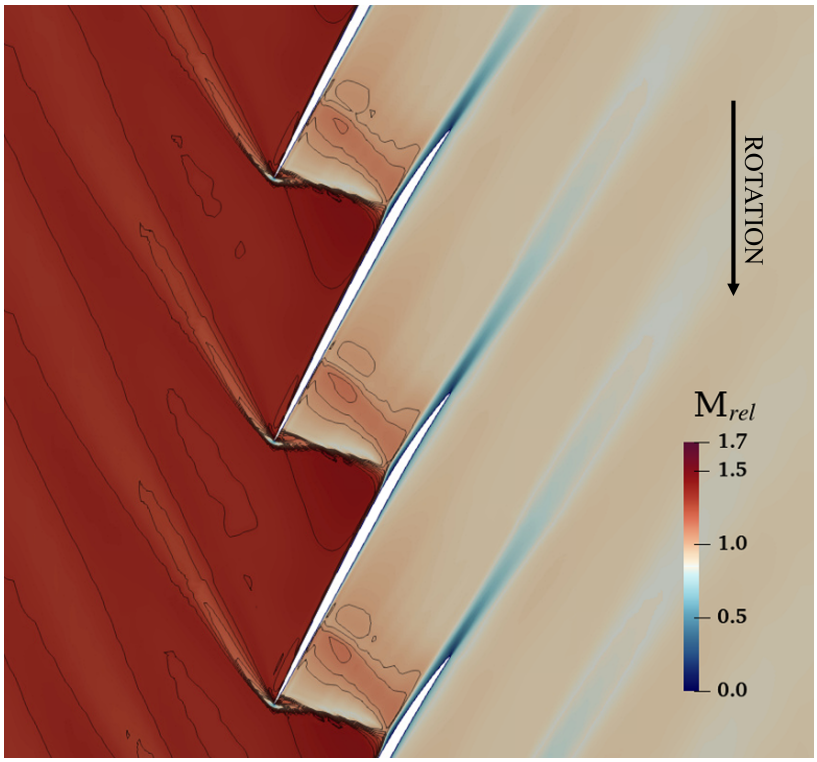

Figure 4: Steady flow results - Relative Mach contours with constant Mach lines at 90% span

surface. The passage shock at 90% span has moved further inside towards the trailing edge when compared to that at at 70% span. This is because the shock is observed—in experiments as well as in our analysis—to be leaning from the inboard span-wise locations towards the tip. The authors have earlier carried out URANS simulation and captured shock buffet at this operating point, details of which can be found in [13].The buffet was a turbulent shock buffet with Re $\approx 3 \times 10^6$ and Strouhal number, $St = \frac{f c_t}{U_{rel}} \approx 0.076$ based on the inlet relative velocity (U_{rel}) and the blade tip chord (c_t), f being the buffet frequency.

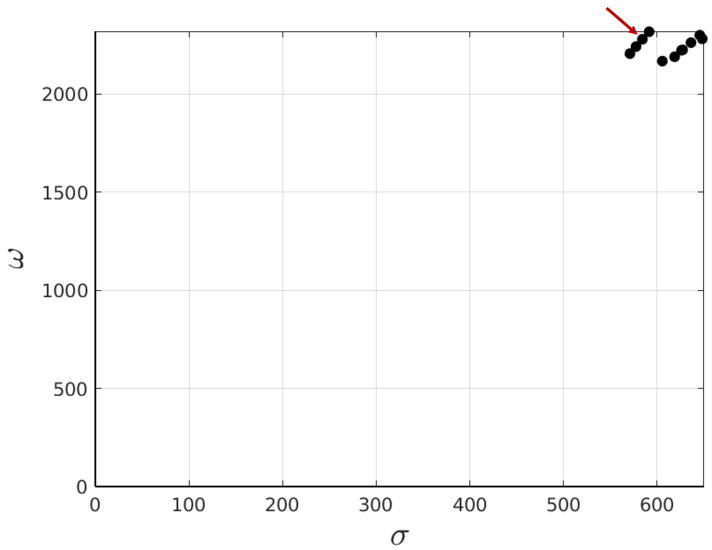

Figure 5: Eigen spectrum of the viscous Jacobian in the vicinity of the buffet frequency

The steady flow solution was taken as the base flow for the global stability analysis. The Jaco-

bians for the convective and viscous conserved variables are extracted from the steady solution using SU2. A few eigenvalues using the method outlined in Sec. 3.2 are evaluated in the vicinity of the imaginary axis and around a real component corresponding to the buffet frequency. Figure 5 shows few eigenvalues for the conserved variable $\rho\tilde{\nu}$, where $\tilde{\nu}$ is the Spalart-Allmaras turbulence variable. The global mode corresponding to $St = 0.072$, for which the eigenvalue is pointed to with a red arrow in Fig. 5, is shown in Fig. 6 for 70% span. Note that this global mode is an unstable mode as it has a positive growth rate and the frequency is reasonably close to the buffet frequency ($St = 0.076$) that was found from the URANS simulation [13]. Energetic streets seem to appear aft the bow shock and near the leading edge of each blade. Disturbances are also seen to be growing from near the foot of the shock aft the the passage shock. Further, the disturbances originating from adjacent blades seem to interact with each other.
Figure 7 shows the unstable global mode corresponding to the considered eigenvalue at 90% span. As this span-wise section is very close to the tip (and shroud), the eigen mode is slightly smeared out than it is at 70% span.
The global stability analysis framework presented here is able to predict the buffet instability reasonably well including the frequency and the modeshape. Based on a steady flow solution, one can predict the unstable buffet mode within a few hours of computation in contrast to unsteady simulations which would usually take weeks of computation time with similar sets of computational resources for the considered testcase. It is observed however that the global stability analysis method presented here has a higher requirement of memory—typically one to two order of magnitude higher, which is also reported in [19]—when compared to that for unsteady flow simulations for the same problem.

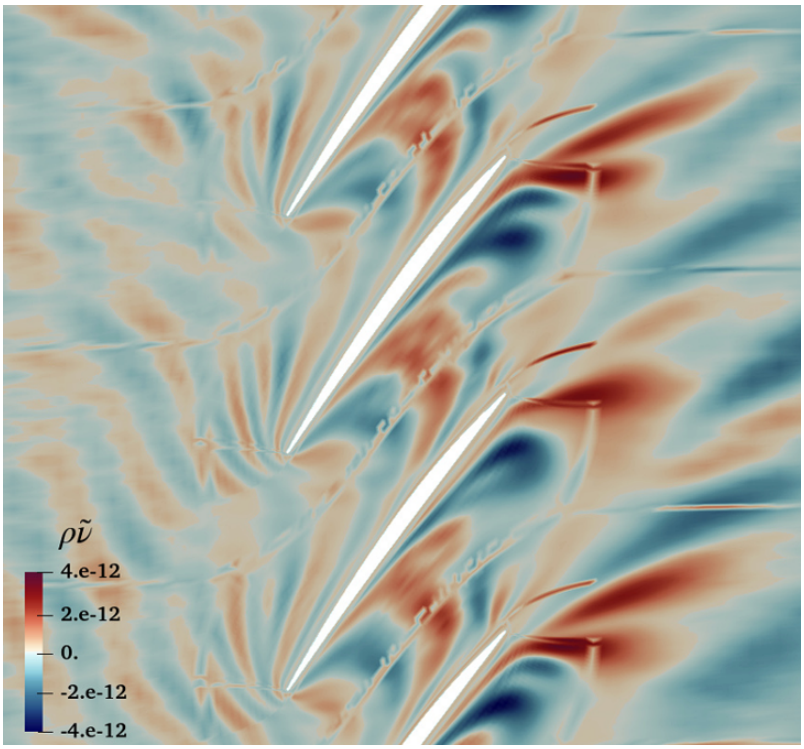

Figure 6: Unstable (buffet) global mode corresponding to $\rho\tilde{\nu}$ at 70% span

5 CONCLUSIONS

A general procedure for carrying out global stability analysis in order to investigate flow instabilities is presented. Global stability analysis is probably employed for the first time for

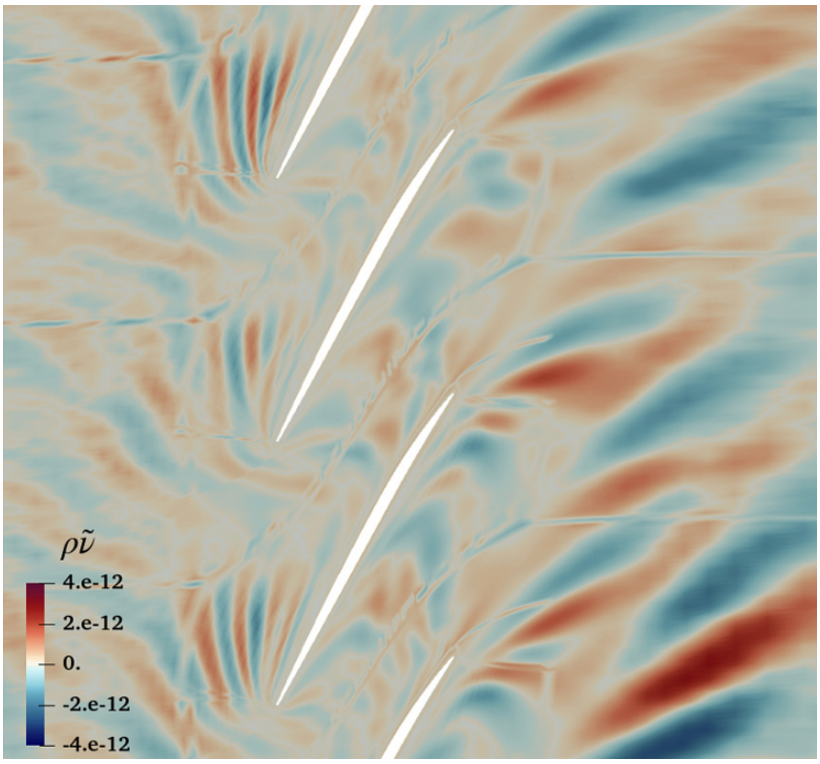

Figure 7: Unstable (buffet) global mode corresponding to $\rho\tilde{\nu}$ at 90% span

predicting shock buffet in a turbomachine. Starting with a steady flow solution as a base flow, transonic shock buffet is predicted for an axial flow fan. The buffet frequency is predicted with in a margin of error of 5% of the value obtained from unsteady simulation. Besides, useful insights of the buffet flow physics are visualized from the unstable global mode. It is shown that, utilizing a steady flow solution as base flow, one can predict the unstable buffet mode within a few hours of computation using global stability analysis in contrast to unsteady flow simulations which would usually take weeks of computation time with similar sets of computational resources for the considered testcase.

6 REFERENCES

[1] Lee, B. H. K. (1990). Transonic buffet on a supercritical aerofoil. *The Aeronautical Journal (1968)*, 94(935), 143–152. doi:10.1017/S0001924000022752.

[2] Jacquin, L., Molton, P., Deck, S., et al. (2009). Experimental study of shock oscillation over a transonic supercritical profile. *AIAA Journal*, 47(9), 1985–1994. doi:10.2514/1.30190.

[3] Hartmann, A., Feldhusen, A., and Schröder, W. (2013). On the interaction of shock waves and sound waves in transonic buffet flow. *Physics of Fluids*, 25(2), 026101. doi:10.1063/1.4791603.

[4] Karnick, P. T. and Venkatraman, K. (2017). Shock–boundary layer interaction and energetics in transonic flutter. *Journal of Fluid Mechanics*, 832, 212–240. doi:10.1017/jfm.2017.629.

[5] Singh, M., Karnick, P. T., and Venkatraman, K. (2022). Transonic buffet and buffeting in the finite span Benchmark Supercritical Wing (BSCW). In *2022 AIAA AVIATION Forum, Chicago, IL, June 27 - July 1, 2022*. doi:10.2514/6.2022-4172.

[6] Lee, B. H. K. (2001). Self-sustained shock oscillations on airfoils at transonic speeds. *Progress in Aerospace Sciences*, 37(2), 147–196. doi:https://doi.org/10.1016/S0376-0421(01)00003-3.

[7] Giannelis, N. F., Vio, G. A., and Levinski, O. (2017). A review of recent developments in the understanding of transonic shock buffet. *Progress in Aerospace Sciences*, 92, 39–84. doi:https://doi.org/10.1016/j.paerosci.2017.05.004.

[8] Gao, C. and Zhang, W. (2020). Transonic aeroelasticity: A new perspective from the fluid mode. *Progress in Aerospace Sciences*, 113, 100596. doi:https://doi.org/10.1016/j.paerosci.2019.100596.

[9] Strazisar, A. J. (1985). Investigation of flow phenomena in a transonic fan rotor using laser anemometry. *Journal of Engineering for Gas Turbines and Power*, 107, 427–435. doi:https://doi.org/10.1115/1.3239743.

[10] Klinner, J., Hergt, A., Grund, A., et al. (2019). Experimental investigation of shock-induced separation and flow control in a transonic compressor cascade. *Experiments in Fluids*, 60(6), 96. doi:https://doi.org/10.1007/s00348-019-2736-z.

[11] Klinner, J., Hergt, A., Grund, S., et al. (2021). High-Speed PIV of shock boundary layer interactions in the transonic buffet flow of a compressor cascade. *Experiments in Fluids*, 62(3), 58. doi:10.1007/s00348-021-03145-3.

[12] Majhi, J. R. and Venkatraman, K. (2023). Prediction and characterization of transonic buffet in an axial-flow fan. In *57th 3AF International Conference on Applied Aerodynamics, Bordeaux, France, March 29 - March 31, 2023*.

[13] Majhi, J. R. and Venkatraman, K. (2023). On the nature of transonic shock buffet in an axial-flow fan. *AIAA Journal*, 61(12), 5390–5403. Doi: `https://doi.org/10.2514/1.J063318`.

[14] Deck, S. (2005). Numerical simulation of transonic buffet over a supercritical airfoil. *AIAA Journal*, 43(7), 1556–1566. doi:https://doi.org/10.2514/1.9885.

[15] Poplingher, L., Raveh, D. E., and Dowell, E. H. (2019). Modal analysis of transonic shock buffet on 2D airfoil. *AIAA Journal*, 57(7), 2851–2866. doi:10.2514/1.J057893.

[16] Zauner, M. and Sandham, N. (2020). Modal analysis of a laminar-flow airfoil under buffet conditions at re = 500000. *Flow Turbul. Combust.*, 104(2-3), 509–532. doi:https://doi.org/10.1007/s10494-019-00087-z.

[17] Moise, P., Zauner, M., and Sandham, N. D. (2022). Large-eddy simulations and modal reconstruction of laminar transonic buffet. *Journal of Fluid Mechanics*, 944(A16). doi:https://doi.org/10.1017/jfm.2022.471.

[18] Crouch, J. D., Garbaruk, A., and Magidov, D. (2007). Predicting the onset of flow unsteadiness based on global instability. *J. Comput. Phys.*, 224(2), 924–940. doi:https://doi.org/10.1016/j.jcp.2006.10.035.

[19] Sartor, C., F.and Mettot and Sipp, D. (2015). Stability, receptivity, and sensitivity analyses of buffeting transonic flow over a profile. *AIAA JOURNAL*, 53(7), 1980–1993. doi:https://doi.org/10.2514/1.J053588.

[20] Timme, S. (2020). Global instability of wing shock-buffet onset. *Journal of Fluid Mechanics*, 885, A37. doi:https://doi.org/10.1017/jfm.2019.1001.

[21] Stewart, G. W. (2001). A krylov-schur algorithm for large eigenproblems. *SIAM Journal of Matrix Analysis and Applications*, 23, 601–614.

[22] Lehoucq, R., Sorensen, D., and Yang, C. (1998). Arpack user's guide: Solution of large-scale eigenvalue problems with implicitly restarted arnoldi methods. *SIAM, Philadelphia*, (6), 1–78.

[23] Strazisar, A. J., Wood, J. R., Hathaway, M. D., et al. (1989). Laser anemometer measurements in a transonic axial-flow fan rotor. *Technical Report NACA-TP-2879*.

[24] Hathaway, M. D. (1986). Unsteady flows in a single-stage transonic axial-flow fan stator row. Tech. Rep. NASA TM 88929.

[25] Palacios, F., Economon, T. D., Aranake, A., et al. (2014). Stanford university unstructured (su2): Analysis and design technology for turbulent flows. In *AIAA SciTech, 52nd Aerospace Sciences Meeting, 13-17 January 2014, National Harbor, Maryland*. doi: 10.2514/6.2014-0243.

[26] Economon, T. D., Palacios, F., Copeland, S. R., et al. (2016). Su2: An open-source suite for multiphysics simulation and design. *AIAA Journal*, 54(3), 828–846. doi:10.2514/1.J053813.

[27] Blazek, J. (2005). *Computational Fluid Dynamics: Principles and Applications*. Oxford: Butterworth–Heinemann.

[28] Hirsch, C. (2007). *Numerical Computation of Internal and External Flows, Volume 1 - Fundamentals of Computational Fluid Dynamics*. Oxford: Butterworth–Heinemann, second ed.

[29] Roe, P. L. (1997). Approximate riemann solvers, parameter vectors, and difference schemes. *Journal of Computational Physics*, 135(2), 252–258. doi:https://doi.org/10.1006/jcph.1997.5705.

[30] Van Albada, G., Van Leer, B., and Roberts, W. (1997). A comparative study of computational methods in cosmic gas dynamics. *Upwind and High-Resolution Schemes, edited by M. Yousuff Hussaini, B. van Leer, and J. Van Rosendale, Springer, Berlin*, 135(2), 95–103. doi:https://doi.org/10.1007/978-3-642-60543-7_6.

[31] Spalart, P. R. and Allmaras, S. R. (1992). A one equation turbulence model for aerodynamic flows. *AIAA Paper*, (92-439). doi:https://doi.org/10.2514/6.1992-439.

[32] Edwards, J. R. and Chandra, S. (1996). Comparison of eddy viscosity transport turbulence models for three-dimensional, shock-separated flowfields. *AIAA Journal*, 34(4), 756–763. doi:10.2514/3.13137.

[33] Grossi, F., Braza, M., and Hoarau, Y. (2014). Modal analysis of transonic shock buffet on 2d airfoil. *AIAA Journal*, 52(10), 2300–2312. doi:10.2514/1.J052873.

[34] Iovnovich, M. and Raveh, D. E. (2014). Numerical study of shock buffet on three-dimensional wings. *AIAA Journal*, 53(2), 449–463. doi:10.2514/1.J053201.

COPYRIGHT STATEMENT